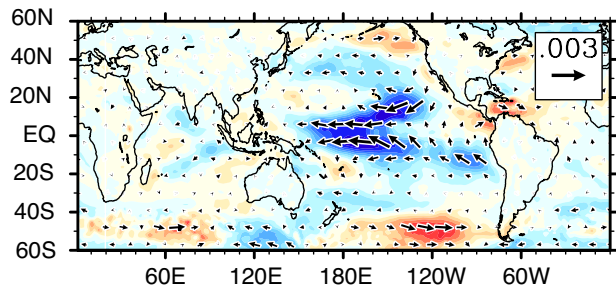


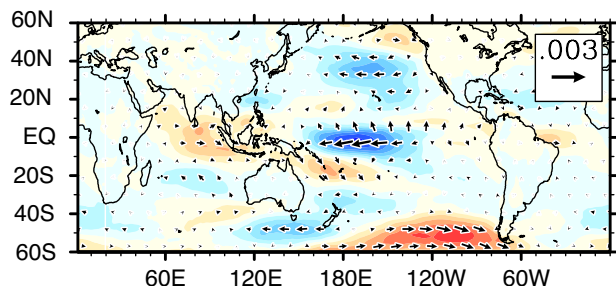
Recent intensification of wind-driven circulation in the Pacific and the ongoing warming hiatus

Matthew H. England^{1,2*}, Shayne McGregor^{1,2}, Paul Spence^{1,2}, Gerald A. Meehl³, Axel Timmermann⁴, Wenju Cai⁵, Alex Sen Gupta^{1,2}, Michael J. McPhaden⁶, Ariaan Purich⁵ and Agus Santoso^{1,2}

(a) Observed wind trends



(b) IPO wind trends



(c) Observed minus IPO wind trends

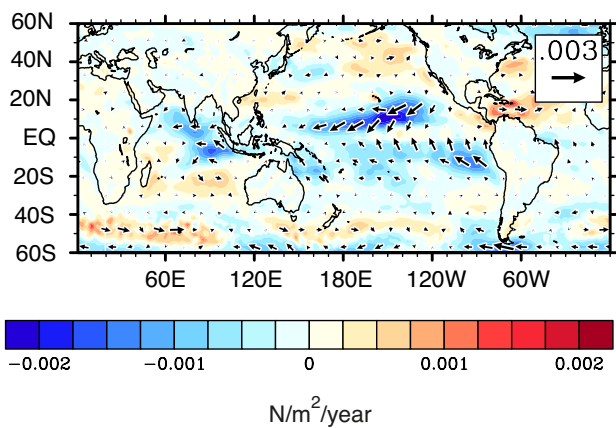


Figure S1 | Observed wind trends during 1992–2011. (a) Observed trends in surface wind stress ($\text{N}/\text{m}^2/\text{year}$) shown as vectors with the strength of the zonal wind stress trend overlaid in colour shading ($\text{N}/\text{m}^2/\text{year}$). Maximum vector scale is indicated. (b) As in (a) but showing the wind stress trends derived from a regression of the Interdecadal Pacific Oscillation (IPO) index. (c) As in (a), but showing the component of the 1992–2011 wind stress trends not accounted for by typical IPO variability (i.e., panel (a) minus panel (b)). The recent observed wind trends (panel (a)) are thus seen to be significantly stronger than those typically associated with the IPO (panel (b)).

¹Australian Research Council (ARC) Centre of Excellence for Climate System Science, The University of New South Wales, Sydney 2052, Australia, ²Climate Change Research Centre, University of New South Wales, Sydney, 2052, Australia, ³National Center for Atmospheric Research, Boulder, Colorado 80307, USA, ⁴International Pacific Research Center, University of Hawaii at Manoa, 1000 Pope Road, Honolulu, Hawaii 96822, USA, ⁵CSIRO Marine and Atmospheric Research, 107-121 Station Street, Aspendale, Victoria 3195, Australia, ⁶National Oceanic and Atmospheric Administration/Pacific Marine Environmental Laboratory, Seattle, Washington 98115, USA. * e-mail: M.England@unsw.edu.au

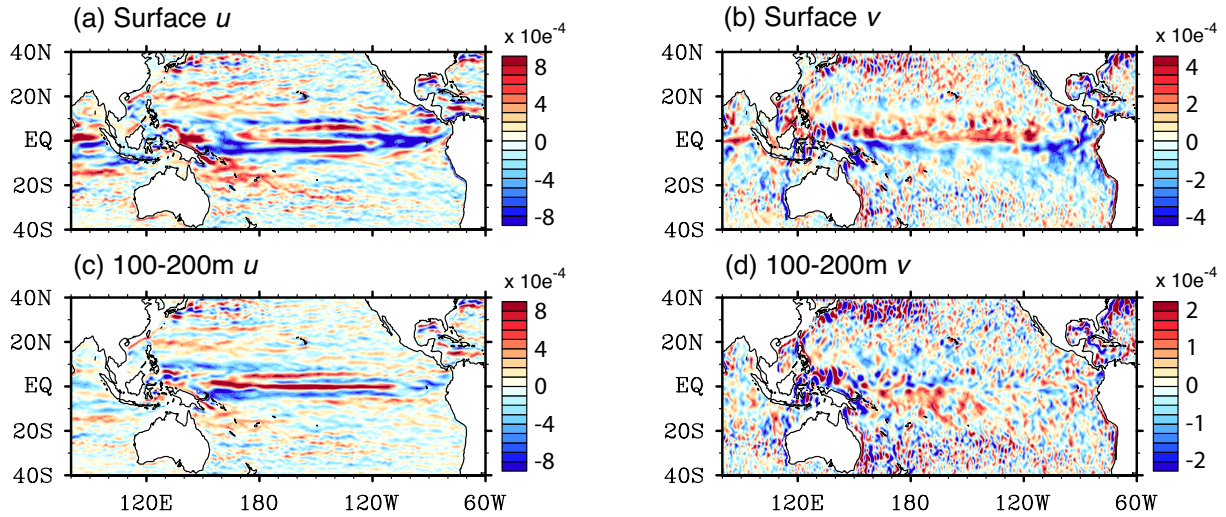
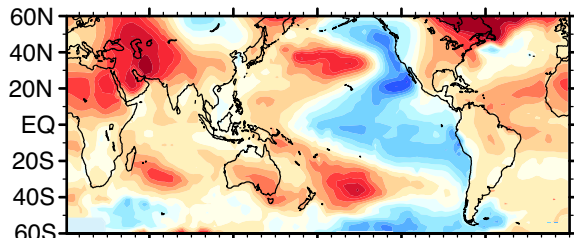
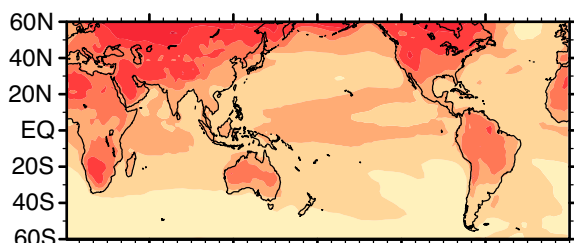


Figure S2 | Recent Pacific basin upper ocean current trends estimated from an ocean reanalysis. The reanalysis product analyzed is the Simple Ocean Data Assimilation (SODA) retrospective analysis of the global ocean¹. Trends are computed over all available SODA data since January 1992 (Jan 1992 - Dec 2008). The ocean current trends are shown at the surface (a,b) and averaged over depths 100-200m (c,d). The ocean velocity trends are shown as two components; (left) zonal velocity trends and (right) meridional velocity trends. Note the different velocity scales used in panels (b,d) to highlight the sign of the meridional velocity trends, including the increased divergence away from the Equator at the surface (panel b) and the recharge of heat toward the Equator at depth (panel d). Outside the tropics, velocity trend estimates are dominated by small-scale noise. Positive values indicate eastward flow (a,c) and northward flow (b,d). Units are m/s/year throughout. The circulation is shown depth averaged over 100-200m as observations are sparse in the ocean interior.

(a) Observed surface air temperature trend



(b) CMIP5 surface air temperature trend



(c) Observed minus CMIP5

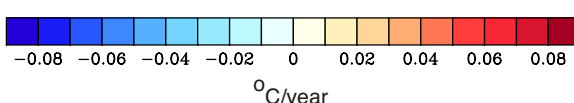
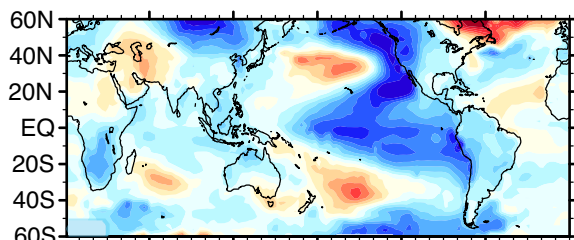


Figure S3 | Observed 1992-2011 trends in air temperature compared to CMIP5 projections. (a) Observed air temperature trends ($^{\circ}\text{C}/\text{year}$) during 1992-2011. (b) As in (a) but showing the air temperature trends in the multi-model ensemble mean of CMIP5 model simulations, using historical forcing up until 2005 followed by the RCP4.5 emissions scenario during 2006-2011. (c) The difference between the observed air temperature trends ($^{\circ}\text{C}/\text{year}$) during 1992-2011 and those of the multi-model ensemble mean of CMIP5 model simulations (i.e., panel (a) minus panel (b)). Subtracting the model estimated air temperature response to anthropogenic forcing (b) from the 1992-2011 trends (a) reveals the Pacific Ocean cooling signature even more strongly (c).

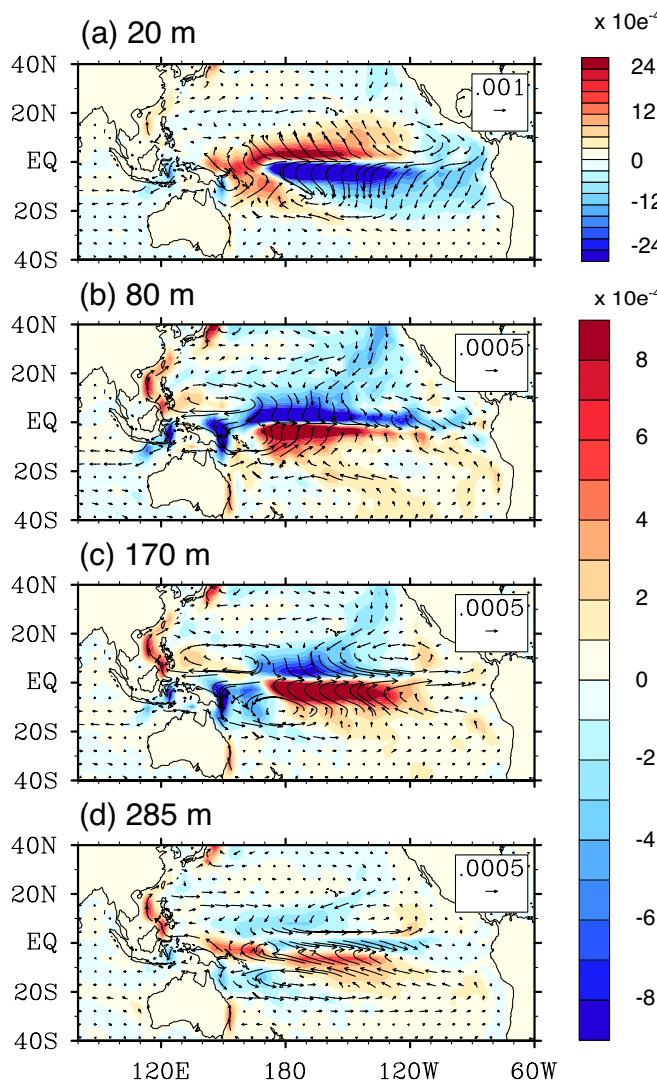


Figure S4 | Model upper ocean circulation anomalies due to the observed 1992-2011 Pacific Ocean wind trends. Vectors show the ocean current trends at depths of (a) 20-m (b) 80-m (c) 170-m and (d) 285-m. The vector scale is indicated in each panel. Overlaid in colour are the meridional velocity trends, with a different colour scale used in panel (a). Units throughout are m/sec/year.

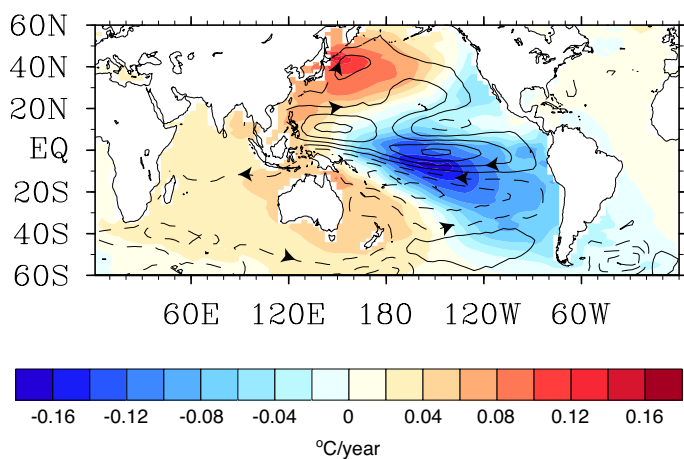


Figure S5 | Model depth-integrated ocean circulation anomalies due to the observed 1992-2011 Pacific Ocean wind trends. Contours show the depth-integrated stream-function trends 1992-2011 spanning the Indian and Pacific Oceans. Contour interval is 0.1 Sv/year, with contours drawn at ± 0.05 , ± 0.15 , ± 0.25 , ± 0.35 , and ± 0.45 Sv/year. Solid (dashed) contours indicate a clockwise (anticlockwise) circulation. Overlaid in colour are the sea surface temperature trends in the model experiment including both historical CO₂ forcing and observed 1992-2011 Pacific Ocean wind trends. Units are $^{\circ}\text{C}/\text{year}$. Apart from the changes in the equatorial circulation and tropical gyres (main text), note also the strengthened Indonesian Throughflow via the Sverdrup relation and Island Rule², and the enhanced Southern Hemisphere ‘supergyre’³, particularly the Indian Ocean component including the Agulhas Current and its retroflection.

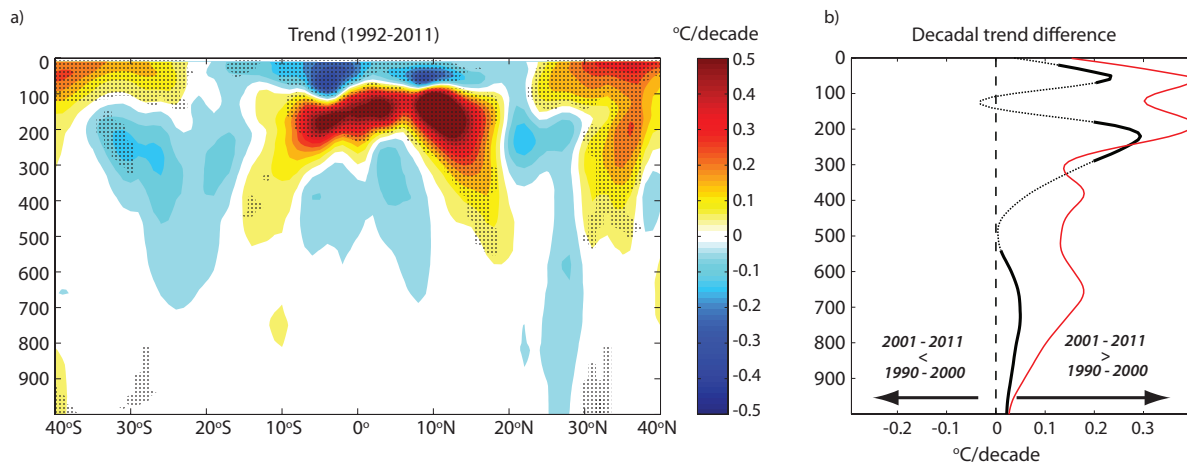


Figure S6 | Zonally-averaged Pacific basin linear trend in potential temperature for the last two decades. (a) Latitude-depth zonal mean temperature trends averaged over five reanalysis products, with stippling used to indicate regions where all five reanalysis products agree on the sign of the trends. (b) Depth profiles of the difference in temperature trends between 2000–2010 compared to 1990–2000, summed over the tropics (10°N – 10°S), averaged over five reanalysis products. Values to the right of the zero dashed line indicate greater warming in the 2000’s compared to the 1990’s. The cooling near the surface at the Equator has persisted since the 1990’s consistent with the 20-year trade wind trends. Solid bold line in panel (b) refers to depths where at least four of the five reanalysis products agree on the sign of the trend difference. The red profile highlights the ORAS4 reanalysis, which also assimilates ERA interim winds. The reanalysis products include: (1) SODA¹ (Jan 1992 – Dec 2008), (2) ECMWF ORAS4^{4,5} (Jan 1992 – Dec 2009), (3) GFDL-ECDA⁶ (Jan 1992 – Dec 2010), (4) ECCO-JPL (Jan 1993 – Dec 2011; <http://ecco.jpl.nasa.gov/>), and (5) NCEP-GODAS⁷ (Jan 1992 – Dec 2011).

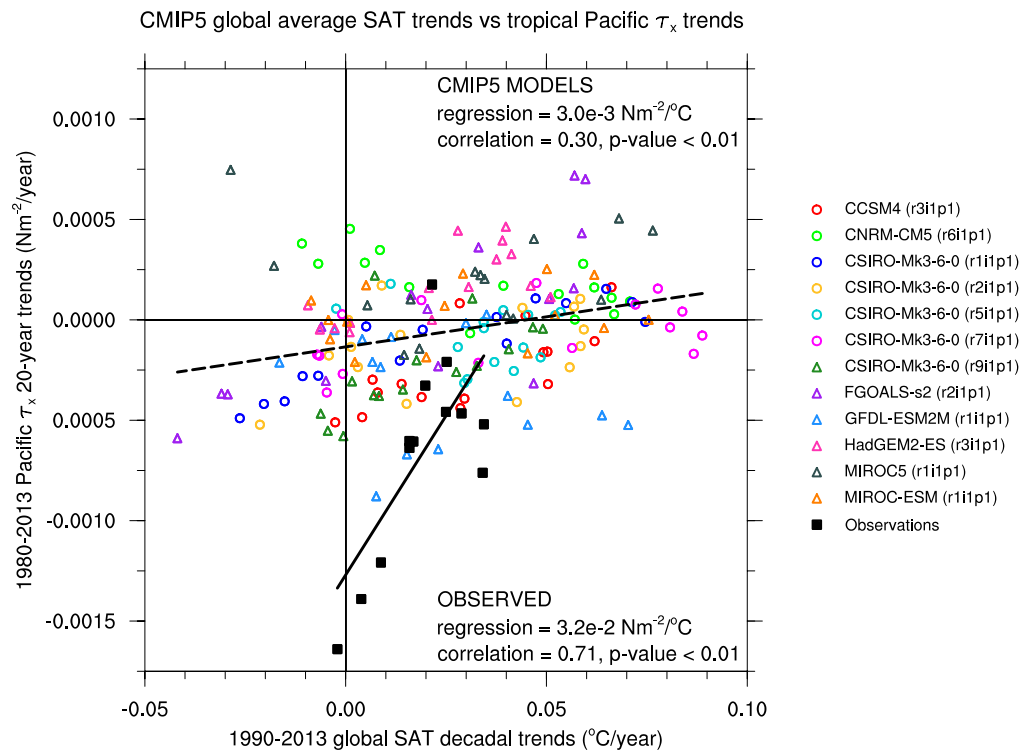


Figure S7 | Twenty-year trends in tropical Pacific winds vs. decadal trends in global surface air temperature (SAT) in observations and models. The global SAT trends are calculated over the last decade of each 20-year wind trend period; so for example, the wind stress trend for the 20-year period 1980–1999 is plotted against the decadal SAT trend from 1990–1999. Model trends are sampled during the period 1980–2013 and observations from 1980–2011. Only those CMIP5 model experiments that, like observations, include at least one hiatus decade during 1990–2013 are shown, as defined by a negative decadal trend in global mean SAT. The wind stress trends are computed over the region 6°N – 6°S and 180° – 150°W , corresponding to where the Interdecadal

Pacific Oscillation (IPO) exhibits maximum regression onto Pacific Ocean wind stress. Wind stress is positive for westerly winds, so negative values indicate acceleration in the Pacific trade winds. A best-fit linear regression is shown separately for both observations and models, along with correlations and an associated significance level (p -value). Of the total of 34 model hiatus decades (SAT trend < 0) simulated post 1990, 26 occur during the last decade of a 20-year positive trend in Pacific trade winds. The observed and model correlations are significant at 99% confidence level. In contrast, the corresponding scatter plot shows little correlation when observed global SAT and Pacific wind trends are compared decade-by-decade. This suggests that the multi-decade Pacific trade wind trend has played a key role in the current hiatus, not just the most recent 10-yrs of Pacific winds.

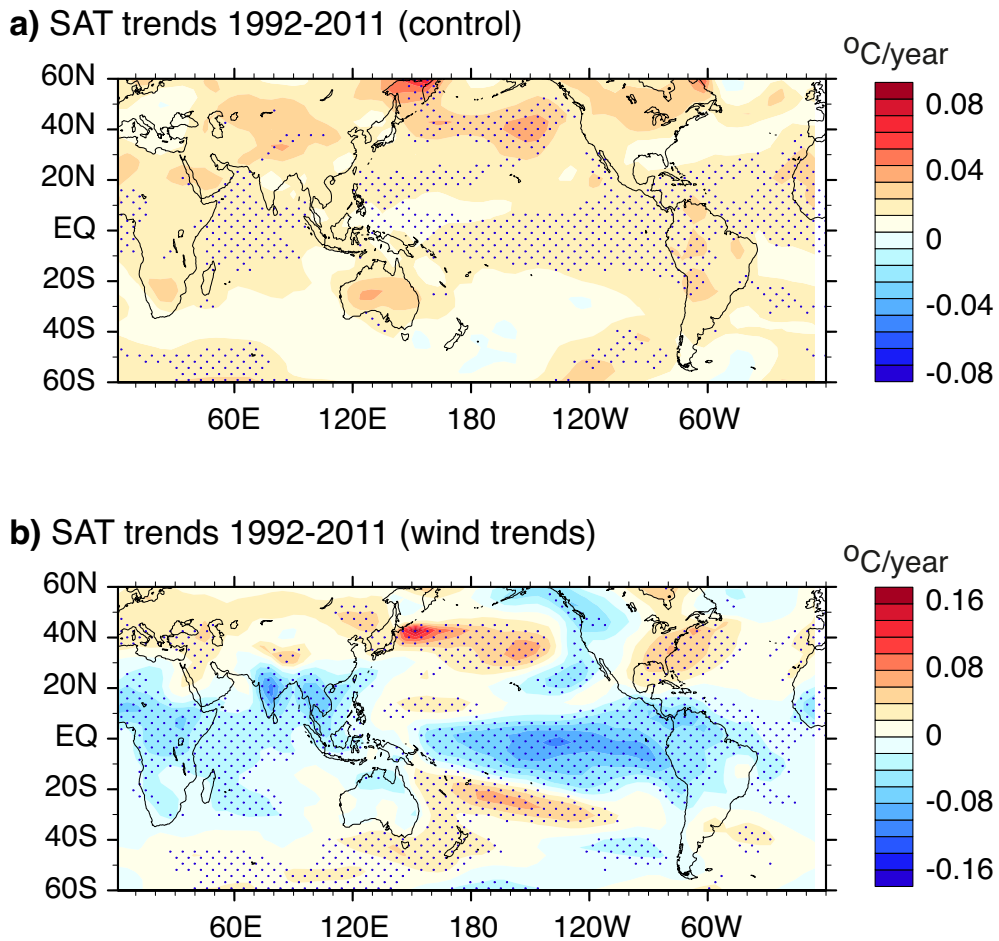


Figure S8 | Average coupled climate model trends in surface air temperature during 1992-2011. (a) In the 12-member control ensemble set wherein the ocean component feels the model's seasonal-mean cycle of Pacific winds over the latitude band 45°N–45°S. Elsewhere the ocean model is forced by the atmospheric GCM, which freely adjusts to the evolving ocean SST field. (b) In the wind trend 12-member ensemble set, which is identical to control, only with the additional wind anomaly imposed corresponding to the observed Pacific wind trends over 1992-2011. As per control, this prescribed wind forcing is limited to the latitude band 45°N–45°S; elsewhere the ocean model is forced by the atmospheric GCM. Stippling indicates where the trend ensemble-means are statistically significant at the 95% confidence level given the linear-regression standard error over the period 1992-2011. The significance of the trend ensemble-mean is evaluated using a two-tailed student t -test by first setting each trend sample to zero (i.e., no trend) if not greater than the 95% linear-regression standard error. The SAT trend patterns in the Pacific sector agree well with the observed (Fig. 2d), although the peak tropical cooling is slightly too large, and there are regions of cooling elsewhere in the tropics that do not match observed, such as in the Indian/Atlantic sectors. This could be due in part to the model's low climate sensitivity (see Methods), although another coupled model study⁸ also simulates cooling over the Indian and Atlantic Oceans during the recent hiatus, which matches observations better for that part of the recent record. Note the different colour scales used above.

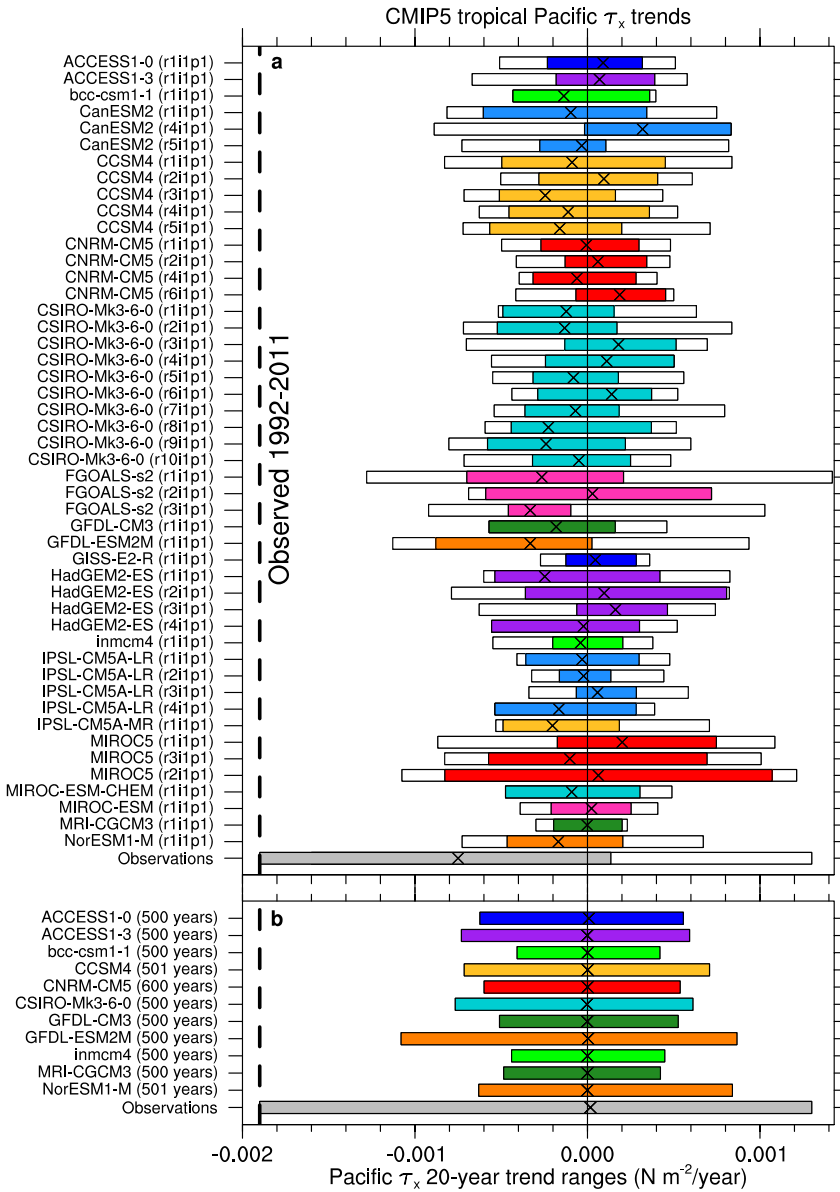


Figure S9 | Observed range in 20-year trends in tropical Pacific trade winds compared to the range captured by CMIP5 models. In the top panel the ranges are shown separately during the periods 1980-2013 (solid fill) and 1860-2013 (solid + unfilled combined) to emphasize the anomalous nature of the recent observed trends. The lower panel shows the corresponding analysis using available preindustrial CMIP5 model runs. The observed and model wind stress trends are computed over the region 6°N - 6°S and 180° - 150°W , corresponding to where the Interdecadal Pacific Oscillation (IPO) exhibits maximum regression onto Pacific Ocean wind stress. Wind stress is positive for westerly winds, so negative values indicate acceleration in the Pacific trade winds. The maximum observed Pacific trade wind acceleration occurs during 1992-2011 (-0.0019 N/m^2 per year), indicated by the vertical dashed line, while the simulated maximum across 48 CMIP5 historical model experiments is generally less than half this magnitude. The symbol x denotes the simulated and observed model mean Pacific trade wind trend during (a) 1980-2012 and (b) all available years (for observed this is 1871-2011). No historical or preindustrial simulation ever captures 20-year Pacific wind trends at the magnitude of the recent observed 1992-2011 trade wind acceleration.

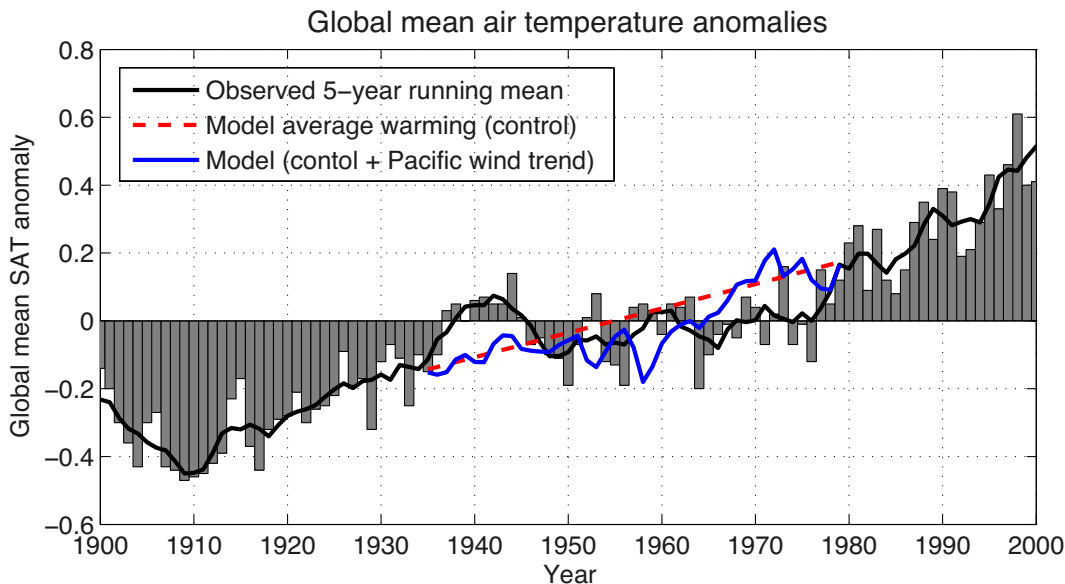


Figure S10 | Twentieth century annual average global air temperature anomalies compared with two model simulations during 1935-1979. Observations are shown as annual values (grey bars) with the 5-year running mean superimposed (black solid line). The model simulation curves show (i) the average warming rate during 1935-1979 in the control experiment with 20th Century CO₂ forcing (red) and (ii) the impact of added wind stress anomalies between 45°S and 45°N in the Pacific Ocean following a regression of the Interdecadal Pacific Oscillation Index onto the ERA-interim wind climatology. The simulation suggests that interdecadal variations in Pacific winds contributed to part of the cooling during the first two decades of the hiatus (1945-1965), but not to the latter part, during 1965-1975, when other processes dominated; foremost the large increase in post World War II aerosols^{9,10}. Thus both cooling due to external forcing (aerosols) and cooling due to variability in the IPO (which may be internally generated or externally forced) appear to have contributed to the mid-20th Century hiatus in surface warming.

References in Supplementary Material

1. Carton, J.A., G.A. Chepurin, X. Cao, and B. Giese, 2000: A Simple Ocean Data Assimilation retrospective analysis of the global ocean 1950-1995. Part I: Methodology. *J. Phys. Oceanogr.*, **30**, 294-309.
2. Godfrey, J. S., 1989: A Sverdrup model of the depth-integrated flow from the world ocean allowing for island circulations. *Geophys. Astrophys. Fluid Dyn.*, **45**, 89–112.
3. Cai, W. J., 2006: Antarctic ozone depletion causes an intensification of the southern ocean super-gyre circulation. *Geophysical Research Letters*, **33**, L03712, 10.1029/2005GL024911.
4. Balmaseda M.A., K. Mogensen, A. Weaver, 2013: Evaluation of the ECMWF Ocean Reanalysis ORAS4. *Quart. J. Roy. Met. Soc.*, in press.
5. Mogensen, K., M.A. Balmaseda, A. Weaver, 2012: The NEMOVAR ocean data assimilation system as implemented in the ECMWF ocean analysis for System 4. ECMWF Technical Memorandum 668. 59 pp.
6. Chang Y.-S., S. Zhang, A. Rosati, T. L. Delworth, and W. F. Stern, 2012: An assessment of oceanic variability for 1960-2010 from the GFDL ensemble coupled data assimilation. *Clim. Dyn.*, **40**, 775-803.
7. Nishida, T, 2011: Validation of the Global Ocean Data Assimilation System (GODAS) data in the NOAA National Centre for Environmental System (NCEP) by theory, comparative studies, applications and sea truth. IOTC-2011-WPB09-11.
8. Kosaka, Y., and S.-P. Xie, 2013: Recent global-warming hiatus tied to equatorial Pacific surface cooling. *Nature*, doi:10.1038/nature12534.
9. Stott, P.A., et al., 2000: External control of 20th century temperature by natural and anthropogenic forcings. *Science*, **290**, 2133–2137.
10. Wilcox L. J., Highwood E. J. and Dunstone N. J., 2013: The influence of anthropogenic aerosol on multi-decadal variations of historical global climate *Environ. Res. Lett.*, **8**, 024033.